The C_4 cycle and beyond: Diverse metabolic adaptations accompany dual-cell photosynthetic functions in Setaria

Paula Calace[1], Tomás Tonetti[2], Ezequiel Margarit[3], Carlos M. Figueroa[2], Carlos Lobertti[1,4], Carlos S. Andreo[1], Mariel C. Gerrard Wheeler[1], Mariana Saigo[1*]

[1] Grupo de Metabolismo del Carbono y Producción Vegetal, Centro de Estudios Fotosintéticos y Bioquímicos (CEFOBI-CONICET), Facultad de Ciencias Bioquímicas y Farmacéuticas, Universidad Nacional de Rosario, Rosario, Argentina.

[2] Instituto de Agrobiotecnología del Litoral (IAL-CONICET), Facultad de Bioquímica y Ciencias Biológicas, Universidad Nacional del Litoral, Santa Fe, Argentina.

[3] Grupo de Calidad de Frutos Cítricos, Bayas y Mejoramiento Forestal, Centro de Estudios Fotosintéticos y Bioquímicos (CEFOBI-CONICET), Facultad de Ciencias Bioquímicas y Farmacéuticas, Universidad Nacional de Rosario, Rosario, Argentina.

[4] Current affiliation: Laboratorio de Patogénesis Bacteriana, Instituto de Biología Molecular y Celular de Rosario (IBR-CONICET), Centro Científico Tecnológico Rosario, Rosario, Argentina.

*corresponding autor: Mariana Saigo. saigo@cefobi-conicet.gov.ar

Paula Calace: calace@cefobi-conicet.gov.ar

Tomás Tonetti: t.tonetti@santafe-conicet.gov.ar

Ezequiel Margarit: margarit@cefobi-conicet.gov.ar

Carlos M. Figueroa: carfigue@fbcb.unl.edu.ar

Carlos Lobertti: lobertti@ibr-conicet.gov.ar

Carlos S. Andreo: carlosandreo@cefobi-conicet.gov.ar

Mariel C. Gerrard Wheeler: gerrard@cefobi-conicet.gov.ar

Highlight

Proteomic and kinetic analyses disclose metabolic strategies involving chloroplastic, mitochondrial and peroxisomal proteins to maintain an optimal performance of the C_4 cycle.

Abstract

C_4 photosynthesis is typically characterised by the spatial compartmentalisation of the photosynthetic reactions into mesophyll (M) and bundle sheath (BS) cells. Initial carbon fixation within M cells gives rise to C_4 acids, which are transported to the BS cells. There, C_4 acids are decarboxylated so that the resulting CO_2 is incorporated into the Calvin cycle. This work is focused on the study of *Setaria viridis*, a C_4 model plant, closely related to several major feed and bioenergy grasses. In the first place, we performed the heterologous expression and biochemical characterization of Setaria isoforms for chloroplastic NADP-malic enzyme (NADP-ME) and mitochondrial NAD-malic enzyme (NAD-ME). The kinetic parameters obtained agree with a major role of NADP-ME in the decarboxylation of the C_4 acid malate in the chloroplasts of BS cells. Besides, mitochondria-located NAD-ME showed regulatory properties that could be important in the context of the operation of the C_4 carbon shuttle. In the second place, we compared the proteomes of M and BS compartments and found 825 differentially accumulated proteins that could support different metabolic scenarios. Most interestingly, we found evidence of metabolic strategies to insulate the C_4 core avoiding the leakage of intermediates by either up-regulation or down-regulation of chloroplastic, mitochondrial and peroxisomal proteins. Overall, the results presented in this work provide novel data concerning the complexity of C_4 metabolism, uncovering future lines of research that will undoubtedly contribute to the expansion of knowledge on this topic.

Keywords

C4 PHOTOSYNTHESIS, GRASSES, MAIZE, MALIC ENZYME, METABOLISM, PROTEOMIC, SETARIA

Abbreviations

3PG 3-phosphoglycerate

AAT aspartate aminotransferase

BS bundle sheath

CA carbonic anhydrase

CCM carbon concentration mechanism

FBP fructose 1,6-bisphosphate

FDR false discovery rate

GDH glutamate dehydrogenase

M mesophyll

Mal malate

MDH malate dehydrogenase

MEP methylerythritol phosphate

MHT multiple hypothesis testing

MVA mevalonic acid

NAD-ME NAD-malic enzyme

NADP-ME NADP-malic enzyme

OAA oxaloacetate

Os *Oryza sativa*

PDHK pyruvate dehydrogenase kinase

PEP phosphoenolpyruvate

PEPC PEP carboxylase

PEPCK PEP carboxyknase

PG 2-phosphoglycolate

PPDK pyruvate orthophosphate dikinase

Pyr pyruvate

RuBP ribulose1,5-bisphosphate

Sb *Sorghum bicolor*

Si *Setaria italica*

Sv *Setaria viridis*

TCA tricarboxylic acid

Zm *Zea mays*

α-KG α-ketoglutarate

Introduction

The challenges brought about by climate change and the future increase of population food and fibre demands require an improvement in crop yields. A deeper understanding of the dynamic response of plants to changing environmental conditions is a key challenge to develop new crop varieties (Bailey-Serres *et al.*, 2019). Furthermore, to enable future production systems to operate more sustainably, it is necessary to increase nitrogen and water-use efficiency (Mueller *et al.*, 2012). The plants that perform C_4 photosynthesis have a higher productivity per crop area, related to an optimised use of water and nutrients, due to the operation of a carbon concentration mechanism (CCM) (Sage, 2004). RuBisCO is a bifunctional enzyme that catalyses the carboxylation of ribulose-1,5-bisphosphate (RuBP) to generate 2 molecules of 3-phosphoglycerate (3PG) and also catalyses the oxygenation of RuBP to generate 3PG and 2-phosphoglycolate (PG). The 3PG pool is used to regenerate RuBP and produce triose phosphate that will fuel carbohydrate biosynthesis. More importantly, PG to be recycled must first be converted to pyruvate (Pyr) by a series of reactions collectively known as photorespiration. This metabolism is energetically costly and, via this pathway, a quarter of the carbons are lost as CO_2. PG production is higher with increasing leaf temperature, a condition that occurs in hot climates, with high irradiation and low evapotranspiration due to stomatal closure. This situation is aggravated by a photoinhibition condition, as NADPH generated in the light reactions accumulates due to a drop in the reductive assimilation of CO_2 in the Calvin cycle. Consequently, in hot and arid environments photosynthetic capacity is reduced by up to 30% (Schulze and Hall, 1982; Jordan and Ogren, 1984; Bauwe *et al.*, 2010).

An increase of carboxylation reactions over oxygenation reactions in the active site of RuBisCO bears the penalty of lower product release rates and hence diminished carboxylation rates (Shih *et al.*, 2016). Consequently, engineering efforts would be more profitable if oriented to develop CCMs that increased the local concentration of CO_2 surrounding RuBisCO (Shih *et al.*, 2016). Plants with C_4 metabolism use, in addition to the enzymes commonly found in C_3 plants, a set of enzymatic activities typically compartmentalised in two cell types that allow them to enrich the RuBisCO environment in CO_2, thus reducing its oxygenase activity (Figure 1, Edwards and Walker, 1983; Hatch, 1987; Sage *et al.*, 2012). First, primary CO_2 fixation occurs in the outer mesophyll (M) compartment, where carbonic anhydrase (CA) converts CO_2 into HCO_3^-, which is used by phosphoenolpyruvate (PEP) carboxylase (PEPC) to carboxylate one molecule of PEP (C_3), thus producing oxaloacetate (OAA, C_4). Unlike RuBisCO, PEPC has no affinity for O_2. Depending on the species, OAA is further transformed into malate (Mal, C_4) or aspartate (Asp, C_4), which are transported to the inner layer of cells known as the bundle sheath (BS). These cells possess several Kranz anatomy characteristics (such as cell walls with reduced gas permeability and positions adjacent to the vascular bundle) which enable them to avoid contact with ambient air (Lundgren *et al.*, 2014). Depending on the prevalent decarboxylating activity in green leaves, C_4 species have been traditionally classified as NADP-malic enzyme (NADP-ME), NAD-malic enzyme (NAD-ME) or phosphoenolpyruvate carboxylase (PEPCK) subtypes (Hatch, 1987). In NADP-ME subtype species, Mal is the C_4 acid transported from M to BS and is decarboxylated in plastids by NADP-ME. In NAD-ME and PEPCK species, Asp is transported between cells and further transformed back to Mal or OAA, which are decarboxylated by NAD-ME or PEPCK in mitochondria or the cytosol, respectively. The C_3 acids generated return to the M, where they are used to regenerate PEP through the action of enzyme pyruvate orthophosphate dikinase (PPDK, Figure 1). The choice of decarboxylase affects many aspects of C_4 photosynthesis beyond the biochemical pathway, such as BS and M ultrastructure, M to BS transport processes, leaf energetics, and photosynthetic efficiency (Hatch, 1987; Drincovich *et al.*, 2011; Ghannoum *et al.*, 2011). A growing body of evidence suggests that C_4 photosynthesis could involve more than one decarboxylase in the same species, which would enable a high photosynthetic performance even in changing environmental conditions (Ludwig, 2016; Schlüter and Weber, 2020). It is currently proposed that C_4 plants could be sub-classified only as NADP- or NAD-ME subtype plants, as there is a clear line of demarcation based on the type of major decarboxylase present, with variable contributions from PEPCK (Furbank, 2011; Wang *et al.*, 2014). Thus, PEPCK could be considered a complementary activity to Mal-decarboxylating enzymes and not as an independent C_4 decarboxylation activity, providing additional mechanisms to balance energy between BS and M under different light conditions and reducing the concentration gradients required to run the C_4 cycle.

The enzymes involved in the C_4 cycle are part of broad protein families, where the other members perform various housekeeping functions, and are therefore referred to as "C_3-type" enzymes. The C_3-type genes are considered to have been the genetic basis for the emergence of the C_4-type variants through duplication and neo-functionalization, which allowed C_4 plant species to gain new enzymes without losing previous functions. High expression levels, response to light, adequate compartmentalisation and optimal structural, catalytic and regulatory properties were the foundations for their new functionality (Sage, 2004; Edwards and Smith, 2010; Maier *et al*, 2011; Saigo *et al*, 2013a, Alvarez *et al*, 2019).

Among grasses (Poaceae), the subfamily Panicoideae includes very important species from an agronomic point of view, as they are used as raw material in the food and biofuel industries. Maize, sorghum and sugarcane all belong to this group and perform NADP-ME-type C_4 photosynthesis. The subclade Paniceae is of particular interest as it includes species of NADP-ME and NAD-ME subtypes, such as *Setaria viridis* (green millet, C_4-NADP-ME), *Setaria italica* (foxtail millet, C_4-NADP-ME) and *Panicum virgatum* (switchgrass, C_4-NAD-ME). *S. viridis* is a small plant, its life cycle lasts between 6 and 9 weeks, it has a small (510 Mb) and sequenced genome (Bennetzen *et al.*, 2012; Mamidi *et al.*, 2020), and robust transformation protocols have been developed for this species (Van Eck, 2018). These technical characteristics, together with its phylogenetic closeness to species of great agronomic importance, have positioned *S. viridis* as a model within the C_4 grasses (Acharya *et al*., 2017; Doust *et al*., 2019). *S. italica* is a very closely related forage crop, since it was developed in China through *S. viridis* domestication.

In this work, we analyse the C_4 pathway of *S. viridis* underlining the metabolic context that supports its photosynthetic process. First, we show that BS enrichment, kinetic performance and regulation of NADP-ME and NAD-ME agree with a role of chloroplastic NADP-ME as the main C_4 decarboxylase and a potential auxiliary role of mitochondrial NAD-ME that would help sustaining the C_4 shuttle. Second, we describe the differential proteomics of chloroplasts, mitochondria and peroxisomes regarding M/BS distribution and discuss the findings in the context of C_4 photosynthesis. A comparison with maize emphasizes the need to characterize the metabolic strategies operating for C_4 cycle in a variety of plant species in order to discriminate core conserved characteristics from species-specific ones. This knowledge provides a deeper understanding of C_4 photosynthesis, which proves essential for facing the challenges involved in plant productivity improvement efforts.

Materials and methods

Plant growth and harvest conditions

Seeds of *Setaria viridis* A10.1 were germinated on plates and then sown on soil. First, seed coats were removed with sandpaper to break the dormancy and to guarantee a high percentage of germination (Van Eck and Swartwood, 2015). Second, seeds were surface-sterilised with a mixture of 1% (w/v) sodium hypochlorite and 0.1% (w/v) Tween-20, and then thoroughly washed with sterile water. Finally, sterile seeds were sown on 0.5X MS-agar plates and incubated at 28°C with irradiance of 120 µmol m^{-2} s^{-1} (16h light/8h dark) for 5 days. Seedlings were transferred to individual 8-cm pots containing Klasmann TSI substrate and irrigated with 1X Hoagland solution. Plants were grown in a Conviron Adaptis A1000 chamber with irradiance of 350 µmol m^{-2} s^{-1} (16h light/8h dark), at 28/22°C (day/night) and 50% relative humidity for 2 weeks. At this stage, plants usually had 8 fully developed leaves and inflorescences were not visible. Leaves 5 and 6 (counting from the bottom of the plant) were harvested at the middle of the photoperiod and immediately used to isolate mesophyll cells (M) and bundle sheath strands (BS).

Separation of M and BS

M cells were isolated using the leaf rolling protocol (Covshoff *et al.*, 2013) with the following modifications. The centre of each leaf was cut in two 5-cm segments and the midrib was removed to generate four segments per leaf. Samples were placed on an ice-cold glass and a plastic rod was rolled twice over the surface of each leaf segment to release the M content, which was rapidly collected using a pipette and dispensed into a 1.5 ml tube on liquid nitrogen.

BS strands were isolated using a method modified from John *et al*. (2014). As mentioned above, leaves were divided into four segments, which were further cut into 2-mm segments. The fragments were placed in isolation buffer (0.33 M sorbitol, 0.3 M NaCl, 0.01 M NaCl, 0.01 M EGTA, 0.01 M dithiothreitol, 0.2 M Tris-HCl pH 9.0, and 5 mM diethylthiophosphoryl chloride), and then pulsed three times for 10 s using a hand blender set at low speed. The suspension was then filtered through a 60-µm mesh, and blending buffer (0.35 M sorbitol, 5 mM EDTA, 0.05 M Tris-HCl pH 8.0, and 0.1% (v/v) 2-mercaptoethanol) was used to return the BS material back into the blender. Homogenization at maximum speed for 1 min followed by filtering was repeated three times. Before the last filtration step, the suspension was strained by a homemade, coarser-pore strainer to obtain the cleaner final sample. Purified BS strands were placed on a paper towel stack to remove excess moisture and then frozen in liquid nitrogen.

In both procedures, four independent isolations from four different batches of leaves were processed as biological quadruplicates.

Total protein extraction

For protein extract preparation, 100 mg of Setaria M and BS samples were pulverised in the presence of 1 ml of extraction buffer, which contains 500 mM Tris-HCl pH 8.0, 50 mM EDTA, 700 mM sucrose, 100 mM KCl, 5% (w/v) poly-vinylpolypyrrolidone, 2% (v/v) 2-mercaptoethanol, and 1% (v/v) complete protease inhibitor cocktail (Roche). Then, 1 ml of phenol equilibrated to pH 8.0 was added and the mixture was incubated on ice and vortexed for 15 min before centrifugation at 10,000 x g for 10 min at 4°C. The organic fraction was collected and five volumes of 100 mM ammonium acetate in methanol were subsequently added. Proteins were left to precipitate for 24 h at -20°C. Samples were centrifuged at 10,000 x g for 20 min at 4°C, and supernatants were removed. Resulting pellets were washed twice with 100 mM ammonium acetate/methanol. Finally, each pellet was suspended in 250 µl of sample buffer (12 mM Tris-HCl pH 6.8, 0.4% (w/v) SDS, 1.5% (w/v) dithiothreitol and 5% (v/v) glycerol) and boiled twice for 5 min. Protein quantification was performed by the Bradford method (Bradford, 1976) using bovine serum albumin as standard.

Protein extracts were checked by Western blot assay in order to verify the correct and efficient separation of cells. For this, M and BS protein samples were run on 10% (w/v) polyacrylamide gels for SDS-PAGE (Laemmli, 1970) and then electroblotted onto nitrocellulose membranes for inmunoblotting according to Burnette (1981). RuBisCO and PEPC antibodies (1:10000, #AS03 037 and 1:1000 #AS09 458, both from Agrisera) were used for the detection of each protein and the assessment of the purity of the samples. Bound-antibodies were located by linking to alkaline phosphatase-conjugated goat anti-rabbit IgG according to manufacturer's instructions (1:10000 dilution, #1721037, Biorad).

Finally, proteins (35 µg per well) were loaded on a 10% (w/v) polyacrylamide gel for SDS-PAGE (Laemmli, 1970) and then run for 1 cm. Bands were visualised by staining with colloidal Coomassie Brilliant Blue G-250, subsequently incubated with a 30% (v/v) methanol solution, and then cut with a sterile scalpel (Leonardi *et al.*, 2015).

Mass spectrometry analysis of protein samples

Samples were digested with trypsin (sequencing grade modified trypsin #V5111, Promega) and cleaned with ZipTips C18 (#ZTC18S096, Merck Millipore). The resulting peptides were analysed by nanoHPLC coupled to a mass spectrometer with Orbitrap technology. A Thermo Scientific EASY-nLC 1000 chromatograph was used to separate protein complexes with a high degree of resolution using a reversed-phase column (Easy-Spray PepMap RSLC C18 column- 3 µm, 100 A, 75 µm x 150 mm; Thermo Scientific) at 35ºC. The injection volume was 4 µl. Aqueous and organic phases were 0.1% (v/v) formic acid in water or in acetonitrile, respectively. A two-step gradient of 5-35% (for 100 min) and 35-100% (for another 5 min) linear increment of the organic phase was used. The flow rate was kept at 200 nl min^{-1} in all steps. An ionizer with a spray voltage of 2.75kV was used to electrospray the eluted peptides. The configuration of the equipment allows peptide identification to be carried out at the same time as the peptides are separated by chromatography, obtaining Full MS (resolution: 70,000 FWHM) and MS/MS (resolution: 17,500 FWHM). A method that performs the highest number of measurement cycles per unit time was used. In each cycle the equipment performs Full MS and then MS/MS to the 15 peaks with the best noise signal in that cycle, with a dynamic exclusion range to prevent the same peak from being fragmented more than once in the same elution peak of the chromatogram.

Identification and abundance estimation of each protein were performed with Proteome Discoverer 2.2 program (Thermo Scientific) run against the *Setaria viridis* UP000298652 (UniProt) database (Mamidi *et al.*, 2020). Protein hits were filtered for high confidence peptide matches with a maximum protein and peptide false discovery rate (FDR) of 1%, calculated by employing a reverse database strategy. Only proteins with a minimum of two peptides detected were considered. Search parameters were adjusted for an error tolerance equal to 0.05 Da for the fragment ions and 10 ppm for the parent ions. Oxidation of methionine residues and carbamidomethylation of cysteine residues were selected as dynamic and static modifications, respectively. To normalize the replicates to each other, a normalization factor was calculated. This was done by first adding up the area of all the proteins in each replicate and then dividing the total area of each replicate by the total area value of an arbitrarily chosen replicate. Subsequently, the area of each individual protein identified for each replicate was divided by the corresponding normalization factor, resulting in the normalised results. Proteins not detected in three or four replicates in BS or M quadruplicates were filtered out before proceeding with the statistical analysis (Supplementary Table 1, Perseus input tab). Statistical analysis (Student's t-test) was performed to compare the abundances of proteins identified in each sample (M and BS). Data was analysed and plotted using Perseus 1.6.6.0 software (Tyanova *et al*., 2016). Three different multiple hypothesis testing (MHT) analyses were performed to evaluate the FDR in the dataset: Benjamini and Hochberg method (Benjamini and Hochberg, 1995), FDR adjusted probability (Reiner *et al*., 2003) and adjusted *p* value using an optimised FDR approach (Storey and Tibshirani, 2003) (Supplementary Table 1, MHT tab).

Bioinformatic analysis

To characterize the proteins of interest, Uniprot identifiers were assigned to those of Phytozome using the *Setaria viridis* v2.1 database (https://phytozome.jgi.doe.gov/pz/portal.html#!info?alias=Org_Sviridis_er). A comprehensive search for genetic information including orthologs assigned to *Arabidopsis thaliana*, *Zea mays*, and *Oryza sativa* was performed.

Functional categories were determined using MapMan X4 and Mercaptor 4.2 tools (Schwacke *et al*., 2019). For this, UniProt identifiers were converted to Ensembl plant identifiers using BioMart 0.7 (Kinsella *et al*., 2011; Howe *et al*., 2020).

The putative subcellular location of each protein was inferred by the identification of its ortholog in proteomic databases of maize chloroplasts (Friso *et al*., 2010), Arabidopsis mitochondria (Fuchs *et al*., 2020) and Arabidopsis peroxisomes (Pan and Hu, 2018). Analysis of primary sequences by TargetP (Almagro Armenteros *et al*., 2019), further confirmed the chloroplastic or mitochondrial location of a number of proteins and expanded the assignment to others (Supplementary Table 1).

Cloning of NADP-ME and NAD-ME isoforms

cDNAs encoding C_4-NADP-ME (Seita.5G134300), NAD-ME1 (Seita.2G322000), and NAD2-ME2 (Seita.9G200600) were amplified by RT-PCR using RNA extracted from *Setaria italica* leaves with Quick-Zol (#RA00201, Kalium Technologies). The concentration and integrity of the preparations were assayed by 2% (w/v) agarose gel electrophoresis. One µg of total RNA was reverse transcribed using M-MLV (#M1705, Promega) and oligodT as primer. Then, amplification was made using Phusion High-Fidelity DNA Polymerase (#F-530XL, Thermo Fisher Scientific) and specific primers. In the case of C_4-NADP-ME, the oligonucleotide pair NdeIC4NADP-for (5´-GTGCAGCATATGGCGGTAGGC-3´) and SalIC4NADP-rev (5´-AGCGGTGACAACGTCGACCAAAAC-3´) was used. NAD-ME1 was amplified using NheINAD1-for (5´-TGCGCTAGCCCCGTCGTCC-3´) and SacINAD1-rev (5´-GCAAACAGAGCTCTCTAGTCTGTC-3´), while NAD-ME2 was amplified using NheINAD2-for (5´-GGCTAGCTGCATCGTGCAC-3´) and XhoINAD2-rev (5´-AGACTCGAGATTTATTTGTCGCTC-3´). The oligonucleotides were designed to introduce restriction sites (underlined) to facilitate subcloning into the expression vector. PCR products were ligated into the pGEMT-easy vector (Promega) and then subcloned into the expression vector pET-28a, which yields recombinant proteins fused to hexahistidine tail (Novagen). Correct cloning was confirmed by capillary electrophoresis sequencing (ABI 3730xl, Macrogen). Vector sequences were deposited in GenBank with the codes MZ463201 (pET28NADME1), MZ463203 (pET28NADME2) and MZ463204 (pET28NADPME).

Expression and purification of recombinant enzymes

The recombinant plasmids containing C_4-NADP-ME, NAD-ME1 and NAD-ME2 inserts were used to transform *Escherichia coli* BL21 (DE3). Bacteria were grown in auto-induction medium in order to induce recombinant expression (Studier, 2005). Fusion proteins were purified using Ni^{2+}-containing His-Bind columns (#71035-4, Novagen). Purified proteins were desalted and concentrated by ultracentrifugation (UFC503096 Amicon) using buffer TMG (50 mM Tris-HCl pH 8.0, 10 mM $MgCl_2$, and 10% (v/v) glycerol). The purity and integrity of the recombinant proteins was analysed by SDS-PAGE revealed with Coomassie dye. Protein concentration was determined using the Bradford method (Bradford, 1976). Purified enzymes were immediately stored in small aliquots at -80°C in buffer TMG.

NADP-ME and NAD-ME activity assays

NADP-ME activity was determined at 30°C in a Jasco V-730 spectrophotometer using a standard reaction mixture containing 50 mM Tris-HCl pH 8.0; 10 mM $MgCl_2$; 0.5 mM $NADP^+$ and 10 mM Mal. NAD-ME activity was measured using a reaction mixture containing 50 mM MES-NaOH pH 6.5; 10 mM $MnCl_2$; 0.5 mM NAD^+ and 10 mM Mal. The optimal pH for each reaction was determined using different buffers as follows: 50 mM sodium acetate-acetic acid (pH 4.5-5.5), 50 mM MES-NaOH (pH 6.0-6.5), 50 mM MOPS-KOH (pH 7.0) and 50 mM Tris-HCl (pH 7.5-8.0-8.9).

Kinetic characterization of the selected enzymes was performed by varying the concentration of one of the substrates (Mal or $NADP^+$/NAD^+), while keeping the level of the other substrate at a fixed and saturating concentration. All kinetic parameters were calculated by fitting to the Hill equation (Detarsio *et al*., 2003; Saigo *et al*., 2013b) in at least three determinations. Since the true substrates of ME are free forms (not forming complexes with metal ions) the data were analysed considering the free concentrations of Mal and $NADP^+$ or NAD^+ in the test medium. The following dissociation constant (*K*d) values for the metal-substrate or metal-cofactor complexes were used: Mg^{2+}-Mal, 28.2 mM; Mn^{2+}-Mal, 20.0 mM; Mg^{2+}-$NADP^+$, 19.1 mM and Mn^{2+}-NAD^+, 12.9 mM (Grover *et al*., 1981).

By assaying different compounds as potential inhibitors or activators of enzyme activity, NADP-ME (or NAD-ME) activity was measured in the presence of either 0.5 mM or 2 mM of each effector (citrate, fumarate, succinate, OAA, fructose 1,6-bisphophate, PEP, α-ketoglutarate, Glu, Ala, and Asp) and non-saturating concentrations of Mal, $NADP^+$ or NAD^+. In the case of CoA and Acetyl-CoA, measurements were performed at a 20 µM concentration of each effector. The inhibition assay of NADP-ME by high Mal concentration was carried out at pH 7.0 (Detarsio *et al*., 2007).

The reductive carboxylation of Pyr (reverse reaction) was tested in various buffer systems (pH 6.5-8.0) containing different concentrations of Pyr (0.1-50 mM), NADPH or NADH (0.1-0.2 mM), $NaHCO_3$ (15-30 mM) and metal cofactors (10 mM $MnCl_2$ or $MgCl_2$).

Results and Discussion

General overview of M and BS proteomes

In order to analyse the proteins enriched in M and BS of Setaria leaves, we separated M cells by the leaf rolling method (Covshoff *et al*., 2013) and BS strands by a method involving blending and filtering procedures (John *et al*., 2014). M and BS proteins were obtained by a phenol-based extraction (Leonardi *et al*. 2015) and exhibited clearly different patterns in Coomassie-stained gels (Supplementary Figure 1A and 1B). To further confirm the quality of the preparations, we verified the enrichment of PEPC (in M) and RuBisCO (in BS) by Western blot (Supplementary Figures 1C and 1D).

According to the mass spectrometry peptide identification and quantification data generated, 1,376 proteins were identified in M and BS total protein samples. In the first step of data processing, 126 proteins were filtered out since they were not detected in three or four replicates in BS or M quadruplicates (Supplementary Table 1). These missing values could be explained by completely random or abundance-dependent effects, which would require further analyses. Statistical analysis of the 1250 remaining proteins shows that 825 proteins (66% of total analysed) are differentially expressed in M and BS cells in a significant way (p-value < 0.05) with less than 10% false positives (Supplementary Table 1), while 489 and 336 proteins are more abundant in M and BS, respectively (Supplementary Table 1, Figure 2A). Furthermore, 68% and 77% of the proteins enriched in BS and M increase their abundance to more than double ($\log_2$(BS/M)>1 and <-1, respectively) supporting the notion that M and BS proteomes are deeply different. The functional categories of the differentially expressed proteins show that many metabolic processes are asymmetrically distributed between M and BS (Figure 2B), further supporting results obtained by previous maize and Setaria transcriptomic analyses (Chang *et al*., 2012, John *et al*., 2014). For example, protein homeostasis and modification, redox homeostasis, the oxidative pentose phosphate pathway, and lipid metabolism are enhanced in M, while more proteins related to Calvin cycle, photorespiration, Pyr oxidation, oxidative phosphorylation, and nucleotide metabolism are present in BS. In addition, functional categories such as light reactions, protein biosynthesis, amino acid metabolism, and solute transport show a similar number of proteins differentially accumulated in M and BS, emphasizing that those processes rely on the cooperation between both compartments (Figure 2B). The comparison of BS/M ratios from our data shows a Pearson's correlation coefficient of 0.725 (p=4.06 E-76) with BS/M ratios obtained by transcriptome analysis (John *et al*., 2014), which indicates good agreement between protein and transcript levels (Supplementary Figure 2).

Among the decarboxylases that can participate in the C_4 cycle, three ME were detected in M and BS proteomes: one chloroplastic NADP-ME (C_4-NADP-ME) and two mitochondrial NAD-ME enzymes (NAD-ME1 and NAD-ME2). The chloroplastic NADP-ME was highly represented in BS proteome, as expected, with an enrichment of 42-fold (log_2FC(BS/M): 5.4) respect to M (Table 1). NAD-ME1 and NAD-ME2 were also more abundant in BS samples (log_2FC(BS/M): 0.83 and 0.87 respectively, Table 1). No PEPCK peptide was detected, which is consistent with the previously reported low level of the transcript encoding this enzyme in M and BS (John *et al.*, 2014; de Oliveira Dal'Molin *et al.*, 2016). Table 1 shows a comparison of the levels of these transcripts and proteins in maize and Setaria. Other C_4 cycle enzymes (such as PEPC and PPDK) were more abundant in M samples, in agreement with their photosynthetic roles and the good quality of the samples (Supplementary Figure 1E and Supplementary Table 1).

In the following sections the kinetic characteristics of NADP-ME and NAD-ME are analysed and discussed in the context of their potential roles. Then, the chloroplastic proteomes of Setaria and maize are compared to highlight their similarities and differences. Finally, the proteomes of mitochondria and peroxisomes of BS and M are analysed in relation to C_4 metabolism.

Chloroplastic NADP-ME is the main decarboxylase in C_4 cycle and probably fulfils additional non-photosynthetic roles in Setaria

In the genomes of *S. viridis* and *S. italica* there is only one gene encoding a plastidic NADP-ME, which is identical in both species. Therefore, we will refer to them as Setaria C_4-NADP-ME. The kinetic analysis of the purified recombinant enzyme shows that C_4-NADP-ME of Setaria shares many characteristics with the maize and sorghum photosynthetic NADP-ME isoforms (Detarsio *et al.*, 2003; Saigo *et al.*, 2013a), such as a high catalytic efficiency and Mal inhibition at pH 7.0 (Figure 3, Table 2). This can be attributed to the conservation of amino acid residues important for the C_4 role, previously identified by crystallographic and site-directed mutagenesis analyses (Supplementary Figure 3, Alvarez *et al.*, 2019). Similarly to maize C_4-NADP-ME (Detarsio *et al.*, 2007), the metabolites tested showed no significant effects on Setaria C_4-NADP-ME activity, while Mal inhibition was the main modulation. This response is important to prevent the overconsumption of Mal under dark conditions, when stromal pH decreases and is close to 7.0 (Saigo *et al.*, 2013b). In maize, the transcript encoding a second plastidic NADP-ME (non-C_4-NADP-ME) has been detected in roots, grains, stems, and leaves where it provides Pyr and NADPH to non-photosynthetic pathways, like plastidic NADP-ME isoforms present in C_3 plants (Gerrard Wheeler *et al*, 2005; Alvarez *et al*, 2013). Considering that Setaria C_4-NADP-ME is the only plastidic isoform encoded in the genome, it probably performs other roles in organs like roots, seeds and leaf M cells. Consistent with this, Setaria C_4-NADP-ME was detected in M protein samples (this study) and non-photosynthetic organs of Setaria (publicly available data, Supplementary Table 2).

Further, the protein sequence of Setaria C_4-NADP-ME also includes residues conserved in non-C_4-NADP-ME from maize, sorghum and rice (Supplementary Figure 3). Additionally, regulatory elements were conserved among these genes (Alvarez *et al*., 2013), which could be essential to fulfil non-photosynthetic roles. Unlike maize, Setaria would represent a case where the neo-functionalization of a C_3-type gene to gain a C_4-type ME function was not accompanied by the retention of the C_3 version.

Mitochondrial NAD-ME2 could collaborate in malate decarboxylation in BS

In plants, NAD-ME isoforms are exclusively mitochondrial while NADP-ME isoforms are present in cytosol and plastids. Together with their 40% identity (on average), NAD- and NADP-dependent enzymes share structural motifs, although they have evolved independently by different events (Tronconi *et al*., 2018). All plant species conserve at least two NAD-dependent isoforms, one α-NAD-ME (NAD-ME1) and one β-NAD-ME (NAD-ME2), which arose by gene duplication late in the evolution of vascular plants (Tronconi *et al*., 2020). NAD-ME1 from *S. italica* and *S. viridis* are identical and the same occurs with their NAD-ME2 proteins, so throughout this work they will be mentioned as Setaria NAD-ME1 and NAD-ME2. The optimal pH and substrate affinities of the purified recombinant enzymes were similar to those reported for Arabidopsis isoforms (Table 3; Tronconi *et al*., 2008). Although Setaria NAD-MEs have lower catalytic constants (more than two times lower, on average), their activity could be higher *in vivo* since they show strong activation by many metabolic effectors (Figures 4A and B). In Arabidopsis, NAD-ME1 and NAD-ME2 are hypothesised to participate in nocturnal respiration, which is supported by a coordinated modulation of the activity by glycolytic and tricarboxylic acid (TCA) cycle intermediates (Tronconi *et al*., 2008 and 2010b). The percentage of identity of NAD-ME1 and NAD-ME2 of Setaria is high (65.8 %) and they are both strongly activated by citrate, α-ketoglutarate (α-KG), succinate, fumarate, fructose 1,6-bisphosphate (FBP) and PEP (Figure 4A and B). In addition, OAA, CoA and Acetyl-CoA are positive modulators of NAD-ME2 (Figure 4B). These regulations indicate that NAD-MEs of Setaria could also be implicated in respiration. Next, we evaluated if Asp, Glu and Ala modulate NAD-ME1 and NAD-ME2 activities. We could not detect any modulation by Asp and Ala, but Glu (2 mM) inhibited NAD-ME2 (Figure 4B). Bacterial and mammalian NAD-ME isoforms are not inhibited by Glu (Teller et al, 1992; Chen et al, 1998; Bologna et al, 2007) and there is no previous report on plant NAD-ME modulation by Glu. Although mitochondrial concentrations of Glu have not been determined, the cytosolic Glu concentration in maize BS has been estimated in 9 mM and Glu has been detected in Setaria leaves at high levels, meaning this regulation could be relevant *in vivo* (Weiner and Heldt, 1992; de Oliveira Dal' Molin et al, 2016; Li et al, 2018). The concerted regulation of NAD-ME2 upregulation by α-KG and downregulation by Glu could be a means to responding to fluctuations in the balance of aminoacids and organic acids. α-KG and Glu are intermediates in many nitrogen balancing reactions mediated by aminotransferases. In the reaction catalysed by aspartate aminotransferase (AAT), Asp is converted to OAA while α-KG is converted to Glu. Then, a high ratio of α-KG/Glu could enhance the production of OAA derived from Asp. After that, malate dehydrogenase (MDH) could reduce OAA to malate. In this way, NAD-ME2 activity and Asp-derived Mal availability would be readily coordinated by the ratio of α-KG/Glu (Figure 4C). Reductive carboxylation of Pyr (reverse reaction) was not detected in our assay conditions neither with NAD-ME1 nor NAD-ME2, in agreement with Arabidopsis enzymes (Tronconi *et al*., 2010a; Badia *et al*., 2017). Therefore, unlike AAT and MDH, which catalyse reversible reactions, NAD-ME1 and NAD-ME2 represent regulatory spots that can have a great influence on organic acid metabolism. Glu and α-KG are also connected by the Glu dehydrogenase (GDH) reaction. In our dataset we could detect that mitochondrial GDH1 and GDH2 were enriched in BS (log_2FC(BS/M): 2.8 and 5.3, respectively; Table 4), which indicates that they could be influencing the ratio of α-KG/Glu in BS, particularly in mitochondria. Although the α-KG/Glu ratio could be participating in the fine tuning of NAD-ME activity in the context of the C_4 cycle, further evidence is needed to prove this hypothesis. Among the mitochondrial metabolite transporters related to C_4 NAD-ME subtypes (Watson-Lazowski *et al.* 2018), PIC (phosphate transporter) was more abundant in BS mitochondria (log_2FC(BS/M): 1.0). Moreover, we found one DTC (dicarboxylate/tricarboxylate transporter, OGC, log_2FC(BS/M): 1.0), homologous to a potential C_4 transporter from *P. virgatum* (Rao and Dixon, 2016) which was significantly enriched in BS mitochondria (log_2FC(BS/M): 1.0). Together, the enrichment of NAD-ME1 and NAD-ME2 in BS, their regulatory properties and the presence of potential C_4 transporters in the envelope of mitochondria suggest that NAD-MEs could participate in the decarboxylation of Mal in the mitochondria in cooperation with chloroplastic NADP-ME. Direct evidence of a species using both NADP-ME and NAD-ME for photosynthesis is limited, but recent works have reported elevated transcript levels for both decarboxylases within the same species (Rao *et al*., 2016; Washburn *et al*. 2017). Dal'Molin et al. (2016) proposed a mixed C_4 decarboxylation mode involving NADP-ME and NAD-ME based on the high abundance of Asp in *S. italica* leaves, which is unusual for NADP-ME species. Nevertheless, Meister et al. (1996) found high levels of Asp in *Flaveria bidentis* (NADP-ME subtype C_4 species) and propose that Asp-derived Mal is decarboxylated in chloroplasts by NADP-ME along with Mal transported from M. Although the same could occur in Setaria it cannot be ruled out that malate transported from M or Asp-derived Mal could also enter mitochondria to supply NAD-ME. Overall, this discussion highlights the limitations of the C_4 models that restrict the carbon circulation through the enzymatic core and rigidly classify the species as NADP-ME, NAD-ME or PEPCK-ME subtypes.

Chloroplastic proteome from Setaria exhibits similarities and differences with maize

In order to organize the data and gain a clearer view, we sub-classified the set of proteins which were significantly and highly enriched in M or BS (*p*-value<0.05, $log_2FC(BS/M)<-1$ or >1) according to their putative subcellular location. We utilised a combination of targeting signals detection strategies by combining bioinformatic tools with the identification of Setaria orthologues of chloroplastic proteins previously detected by a proteomic approach in maize (Friso *et al*., 2010). This strategy helped us visualize the main differences in the metabolic demands of M and BS cells in Setaria. We were able to assign 124 chloroplastic proteins in M and 163 in BS (Supplementary Table 1). Maize proteomics was restricted to the study of chloroplastic proteins, and identified 246 proteins in M and 118 proteins in BS (Friso *et al.*, 2010).

In C_4 species, BS chloroplasts hold much of the photosynthetic machinery since most carbon assimilation steps operate almost exclusively in these organelles. In the NADP-ME subtype, the high amount and catalytic proficiency of chloroplastic NADP-ME provides CO_2 and NADPH to the Calvin cycle. ATP is generated by cyclic electron transport around PSI and the trioseP/PGA shuttle supplies the NADPH needed for carbon assimilation. The chloroplastic proteomes of M and BS in maize provided strong experimental support for a number of specialised BS and M metabolic functions, including starch biosynthesis (BS), the methylerythritol phosphate (MEP) pathway for isoprenoid biosynthesis (M), nitrogen assimilation (M) and the initial steps of sulfur assimilation (BS), among others (Friso *et al*., 2010). Here, we obtained evidence that shows that many M- and BS-specific metabolic functions are conserved in Setaria chloroplasts. However, some other functions are markedly different from maize (Supplementary Table 1). The comparison of the distribution and level of chloroplastic proteins of maize and *S. viridis* shows a Pearson's correlation coefficient of 0.355 (p = 1.09 E-10, Supplementary Figure 4). Among the 310 proteins included in this analysis, 220 were detected in the same sample compartment (M or BS) in both species (Supplementary Table 1). For example, 1-deoxy-D-xylulose 5-phosphate reductase (DXR), the second enzyme of the MEP pathway, accumulates at higher levels in M than in BS chloroplasts (Table 4). This can be attributed to a high demand of tocopherol, needed to protect membranes from oxidative damage derived from linear electron transport in M chloroplasts (Soll *et al*., 1983; Lichtenthaler *et al*., 1997). On the other hand, 94 maize M-enriched proteins were identified as BS-enriched in Setaria. For example, many enzymes involved in chlorophyll biosynthesis (glutamate-1-semialdehyde-2,1-aminomutase, Mg-protoporphyrin IX chelatase, Mg-protoporphyrin O-methyltransferase and Mg-protoporphyrin IX monomethyl ester cyclase) and the shikimate pathway for aromatic amino acids biosynthesis (3-dehydroquinate synthase, 3-dehydroquinate dehydratase and shikimate kinase) are enhanced in Setaria BS chloroplasts (Table 4), in contrast to what occurs in maize, where these pathways are enriched in M chloroplasts (Friso *et al*., 2010).

Chorismate synthase and arogenate dehydratase, the enzymes which catalyze the last steps in chorismate and phenylalanine biosynthesis respectively, are also up-regulated in Setaria BS (Table 4), but their presumably chloroplastic location could not be verified in this work. The weak correlation of M and BS chloroplast proteins of maize and *S. viridis* was already noted when comparing Setaria RNA-Seq and maize proteomics (John *et al.*, 2014). These observations could be attributed to species-related divergences and could also point towards differences between leaf tip (Friso *et al.*, 2010) and middle blade tissues (this study). Detailed studies of the proteomic, transcriptomic and metabolomic patterns along the maize leaf have shown that metabolism largely varies from the heterotrophic base (sink) to the photosynthetic tip (source) (Majeran *et al.*, 2010; Pick *et al.*, 2011). While the region closer to the base is characterised by the biosynthesis of lipids, cell wall, lignins and isoprenoids (MVA pathway) to support the expansion of the cells, the tip is engaged in highly efficient photosynthetic C_4 cycle reactions, which provide carbon compounds to other tissues. This distribution of roles helps avoiding interferences between photosynthesis and other metabolisms. In this work, we analysed the central portion of *S. viridis* leaf, where we propose alternative strategies are used to maintain the metabolic homeostasis of the cells. In this sense, a lower activity of the shikimate pathway in M would prevent the consumption of PEP, thus avoiding an interference with the C_4 cycle.

The pattern of distribution of mitochondrial proteins between BS and M reveals metabolic strategies necessary to avoid interference with C4 cycle carbon flow

Following a strategy similar to the one applied with chloroplastic proteins, we could detect 22 putative mitochondrial proteins significantly enriched in M and 30 mitochondrial proteins enriched in BS (Fuchs *et al.*, 2020). In M, enzymes involved in the degradation of leucine (isovaleryl-CoA-dehydrogenase, 3-methylcrotonyl-CoA carboxylase) and phenylalanine (fumarylacetoacetate hydrolase) seem to be present at higher levels (Table 4). Despite the fact that catabolic pathways for both amino acids are completely different, both contribute to the pool of Acetyl-CoA independently of pyruvate oxidation, thus avoiding interference with C_4 cycle carbon flow. In BS mitochondria, there are higher levels of TCA cycle enzymes and TCA cycle-related enzymes (isocitrate dehydrogenase 1, fumarase 2, Glu dehydrogenase 1 and 2), phosphate and carbon compound transporters (phosphate transporter 3;1, mitochondrial substrate carrier family protein), electron transport chain and oxidative phosphorylation components (delta subunit of ATP synthase, ubiquinol-cytochrome C reductase iron-sulfur subunit, plant uncoupling mitochondrial protein 1, cytochrome bd ubiquinol oxidase 14 kDa subunit) and redox response proteins (manganese superoxide dismutase 1, peroxiredoxin IIF), which is characteristic of an active oxidative metabolism (Table 4). However, the accumulation of pyruvate dehydrogenase kinase (PDHK, Table 4) in this organelle implies that the pyruvate dehydrogenase complex could be inhibited, raising the question of which substrate is oxidised by the TCA cycle. In this regard, it is important to recall that in plants the enzymatic activities of the TCA cycle can operate in diverse metabolic contexts in non-cyclic fashions, resembling more an organic acid network deeply connected with the cytosol than a closed mitochondrial cycle (Sweetlove *et al.*, 2010). Considering that in BS chloroplasts pyruvate consuming pathways could be active (such as beta-reduction for fatty acid and isoprenoid biosynthesis) at least at a low rate, the decarboxylation of malate in BS mitochondria catalysed by NAD-ME isoforms would provide an alternative route to supply pyruvate for photosynthetic PEP recycling in M. The enrichment of PDHK in mitochondria of BS has been pointed out as a NAD-ME C_4 pathway marker, since avoiding the leakage of intermediates from the C_4 core to other metabolic routes is critical for the robustness of C_4 cycle functioning (Bräutigam *et al*, 2014). In this work, we present evidence of several strategies that could operate in Setaria leaves to uncouple the C_4 cycle from other pathways.

Peroxisomal production of Acetyl-CoA is enhanced in M

In C_3 plants, peroxisomes collaborate with chloroplasts and mitochondria in the recycling of PG carbon by photorespiration among many other metabolic functions, such as fatty acid β-oxidation and phytohormone biosynthesis (see Kao *et al.*, 2018 for a review). In C_4 plants photorespiration has been minimised and restricted to BS, the site where PG is produced. To further investigate the metabolic routes that operate in peroxisomes of M and BS, we identified a group of putative peroxisomal proteins by retrieving the orthologues of Arabidopsis peroxisomal proteins from the set of proteins enriched in Setaria M or BS (Pan and Hu, 2018). In the M-enriched set, 26 peroxisomal proteins were identified, while none were identified in the BS-enriched group (Supplementary Table 1). The functional categories of M proteins indicate active Acetyl-CoA production by β-oxidation of fatty acids (acyl-CoA oxidase 1, 3-hydroxyacyl-CoA dehydrogenase, 3-ketoacyl-CoA thiolase 3), which would be the main source of H_2O_2 instead of photorespiration (Table 4). This elevated production of H_2O_2 can be compensated by the upregulation of catalases 1 and 2 and the ascorbate-glutathione redox system (glutathione reductase, monodehydroascorbate reductase 1) in order to protect the cell from oxidative damage (Table 4). Acetyl-CoA thiolase and isopentenyl diphosphate (IPP) isomerase accumulated at higher levels in M peroxisomes than in BS (Table 4) thus potentially providing a higher level of IPP and dimethylallyl pyrophosphate (DMAPP), to feed biosynthesis of terpenoids and phytosterols through the mevalonate (MVA) pathway (Vranová *et al.*, 2013). Acetyl-CoA production probably does not fuel gluconeogenesis, since the glyoxylate pathway diminishes as seedlings mature (Titus and Becker, 1985) and Mal synthase was not detected in our data. The accumulation of malate dehydrogenase (MDH) and citrate synthase in peroxisomes (Table 4) and ATP-citrate lyase in the cytosol of M (Sevir.8G254100, $\log_2FC(BS/M)$: -1.54; Supplementary Table 1) could be supporting the active export of Acetyl-CoA by the citrate shuttle (Table 4). In the cytosol, Acetyl-CoA is able to feed other biosynthetic routes. For example, the acetylation of serine using Acetyl-CoA is the first step to cysteine biosynthesis, which could be enhanced in M since the second enzyme of the pathway is enriched in this compartment (O-acetylserine (thiol) lyase, Sevir.3G415300, $log_2FC(BS/M)$: -2.5; Supplementary Table 1). Acetyl-CoA could be further incorporated to the nucleus in order to support the acetylation of histones. In this sense, it was recently found that peroxisomal β-oxidation regulates histone acetylation and DNA methylation in Arabidopsis (Wang *et al.*, 2019). This, together with the finding that the acetylation of histones in PEPC and ME promoters modulates the expression of these genes (Heinmann *et al.*, 2013), discloses a possible relationship between peroxisomal metabolism and epigenetics in defining expression patterns in M and BS.

Concluding remarks

The data outlined in this work indicates that C_4-NADP-ME in Setaria display kinetic characteristics relevant for C_4 function. Unlike what occurs in maize, in Setaria this isoform would also fulfil non-photosynthetic functions, being that it is the only plastidic isoform encoded in this plant's genome. On the other hand, enrichment of NAD-ME and organic acid transporters in Setaria BS mitochondria together with kinetic regulation of NAD-ME, suggest that Mal decarboxylation in BS mitochondria may be active in parallel to its chloroplastic decarboxylation catalysed by C_4-NADP-ME (Figure 5). Nevertheless, the contribution of Mal decarboxylation in the mitochondria to *in vivo* C_4 carbon fixation has not been determined and deserves further exploration.

Based on comparative proteomics of M and BS, we found evidence of several strategies to avoid the leakage of C_4 intermediates. The Pyr generated in the mitochondria of BS would not be oxidised to form Acetyl-CoA, while in M several Pyr-independent pathways of Acetyl-CoA generation would be enhanced. In both cases, the Pyr pool would be preserved to maintain the C_4 shuttle. Additionally, in M chloroplasts down-regulation of the shikimate pathway would reserve PEP molecules for primary carboxylation by PEPC (Figure 5).

C_4 leaves present transversal (M-BS) and longitudinal (base-tip) metabolic gradients that need to be finely coordinated in order to achieve high carbon assimilation rates. In those segments where there is an overlapping of several pathways, a fine regulation is essential for guaranteeing metabolic homeostasis. Although a great amount of multi-omic studies are currently approaching this subject, we understand a deeper research into the key post-translational modification reactions and enzymatic regulatory mechanisms involved is also required.

Data availability statement

All data supporting the findings of this study are available within the paper and within its supplementary materials published online.

Acknowledgements

EM, CMF, CSA, MCGW, and MS belong to the Researcher Career of National Council of Scientific and Technical Research (CONICET). PC and TT are fellows of the same institution. This work was financially supported by the National Agency for Promotion of Science and Technology grants to CSA (PICT-2014-2556) and MS (PICT-2019-02890). CMF is funded by the National Agency for Promotion of Science and Technology (PICT-2018-00865) and the Max Planck Society (Partner Group for Plant Biochemistry). The authors thank Silvia Moreno and María Pía Valacco (CEQUIBIEM) for technical assistance in the proteomic analysis and Celina Galles for the improvement of the manuscript.

Author contributions

CMF, CSA, MCGW, and MS designed the concept and planned the experiments of this study. PC, TT, CMF, and MS performed the experiments regarding M and BS separation, protein extraction, and sample preparation for mass spectrometry. PC, EM, and MS were involved in the bioinformatic analysis. PC, CL, MCGW, and MS carried out the cloning, expression, and kinetic characterization of the recombinant enzymes. PC, EM, CMF, MCGW, and MS were involved in the analysis and interpretation of the results. MS and PC, in collaboration with all the other authors, wrote and edited the manuscript.

Data Availability Statement

All data supporting the findings of this study are available within the paper and within its supplementary materials published online.

References

Acharya BR, Roy Choudhury S, Estelle AB, Vijayakumar A, Zhu C, Hovis L, Pandey S (2017) Optimization of phenotyping assays for the model monocot *Setaria viridis*. Front. Plant Sci. 8: 2172. https://doi.org/10.3389/fpls.2017.02172

Almagro Armenteros, J. J., Salvatore, M., Emanuelsson, O., Winther, O., von Heijne, G., Elofsson, A., & Nielsen, H. (2019). Detecting sequence signals in targeting peptides using deep learning. *Life science alliance*, *2*(5), e201900429. https://doi.org/10.26508/lsa.201900429

Alvarez, C. E., Bovdilova, A., Höppner, A., Wolff, C. C., Saigo, M., Trajtenberg, F., Zhang, T., Buschiazzo, A., Nagel-Steger, L., Drincovich, M. F., Lercher, M. J., & Maurino, V. G. (2019). Molecular adaptations of NADP-malic enzyme for its function in C_4 photosynthesis in grasses. *Nature plants*, *5*(7), 755–765. https://doi.org/10.1038/s41477-019-0451-7

Alvarez, C. E., Saigo, M., Margarit, E., Andreo, C. S., & Drincovich, M. F. (2013). Kinetics and functional diversity among the five members of the NADP-malic enzyme family from Zea mays, a C4 species. *Photosynthesis research*, *115*(1), 65–80. https://doi.org/10.1007/s11120-013-9839-9

Badia MB, Mans R, Lis AV, Tronconi MA, Arias CL, Maurino VG, Andreo CS, Drincovich MF, van Maris AJ, Gerrard Wheeler MC (2017) Specific *Arabidopsis thaliana* malic enzyme isoforms can provide anaplerotic pyruvate carboxylation function in *Saccharomyces cerevisiae*. FEBS J. 284: 654–665. https://doi.org/10.1111/febs.14013

Bailey-Serres, J., Parker, J. E., Ainsworth, E. A., Oldroyd, G., & Schroeder, J. I. (2019). Genetic strategies for improving crop yields. *Nature*, *575*(7781), 109–118. https://doi.org/10.1038/s41586-019-1679-0

Bauwe, H., Hagemann, M., & Fernie, A. R. (2010). Photorespiration: players, partners and origin. Trends in plant science, 15(6), 330–336. https://doi.org/10.1016/j.tplants.2010.03.006

Benjamini, Y., Drai, D., Elmer, G., Kafkafi, N., & Golani, I. (2001). Controlling the false discovery rate in behavior genetics research. *Behavioural brain research*, *125*(1-2), 279–284. https://doi.org/10.1016/s0166-4328(01)00297-2

Bennetzen, J. L., Schmutz, J., Wang, H., Percifield, R., Hawkins, J., Pontaroli, A. C., Estep, M., Feng, L., Vaughn, J. N., Grimwood, J., Jenkins, J., Barry, K., Lindquist, E., Hellsten, U., Deshpande, S., Wang, X., Wu, X., Mitros, T., Triplett, J., Yang, X., … Devos, K. M. (2012). Reference genome sequence of the model plant Setaria. Nature biotechnology, 30(6), 555–561. https://doi.org/10.1038/nbt.2196

Bradford M. M. (1976). A rapid and sensitive method for the quantitation of microgram quantities of protein utilizing the principle of protein-dye binding. *Analytical biochemistry*, *72*, 248–254. https://doi.org/10.1006/abio.1976.9999

Bräutigam, A., Schliesky, S., Külahoglu, C., Osborne, C. P., & Weber, A. P. (2014). Towards an integrative model of C4 photosynthetic subtypes: insights from comparative transcriptome analysis of NAD-ME, NADP-ME, and PEP-CK C4 species. Journal of experimental botany, 65(13), 3579–3593. https://doi.org/10.1093/jxb/eru100

Burnette W. N. (1981). "Western blotting": electrophoretic transfer of proteins from sodium dodecyl sulfate--polyacrylamide gels to unmodified nitrocellulose and radiographic detection with antibody and radioiodinated protein A. Analytical biochemistry, 112(2), 195–203. https://doi.org/10.1016/0003-2697(81)90281-5

Covshoff, S., Furbank, R. T., Leegood, R. C., & Hibberd, J. M. (2013). Leaf rolling allows quantification of mRNA abundance in mesophyll cells of sorghum. Journal of experimental botany, 64(3), 807–813. https://doi.org/10.1093/jxb/ers286

de Oliveira Dal'Molin, C. G., Orellana, C., Gebbie, L., Steen, J., Hodson, M. P., Chrysanthopoulos, P., Plan, M. R., McQualter, R., Palfreyman, R. W., & Nielsen, L. K. (2016). Metabolic Reconstruction of Setaria italica: A Systems Biology Approach for Integrating Tissue-Specific Omics and Pathway Analysis of Bioenergy Grasses. Frontiers in plant science, 7, 1138. https://doi.org/10.3389/fpls.2016.01138

Detarsio E, Alvarez CE, Saigo M, Andreo CS, Drincovich MF (2007) Identification of domains involved in tetramerization and malate inhibition of maize C4-NADP-malic enzyme. J. Biol. Chem. 282: 6053–6060. https://doi.org/10.1074/jbc.M609436200

Detarsio E, Wheeler MC, Campos Bermúdez VA, Andreo CS, Drincovich MF (2003) Maize C4 NADP-malic enzyme. Expression in Escherichia coli and characterization of site-directed mutants at the putative nucleoside-binding sites. J. Biol. Chem. 278: 13757–13764. https://doi.org/10.1074/jbc.M212530200

Drincovich MF, Lara MV, Maurino VG, Andreo CS (2011) C4 decarboxylases: different solutions for the same biochemical problem, the provision of CO2 to Rubisco in the bundle sheath cells. In: C4 photosynthesis and related CO2 concentrating mechanisms. Raghavendra AS, Sage RF (eds.), Springer Netherlands: 277–300. https://doi.org/10.1007/s11120-013-9879-1

Doust, A. N., Brutnell, T. P., Upadhyaya, H. D., & Van Eck, J. (2019). Editorial: *Setaria* as a model genetic system to accelerate yield increases in cereals, forage crops, and bioenergy grasses. *Frontiers in plant science*, *10*, 1211. https://doi.org/10.3389/fpls.2019.01211

Edwards, E. J., & Smith, S. A. (2010). Phylogenetic analyses reveal the shady history of C4 grasses. *Proceedings of the National Academy of Sciences of the United States of America*, *107*(6), 2532–2537. https://doi.org/10.1073/pnas.0909672107

Edwards, GE and Walker, DA (1983). C3, C4: Mechanism, and Cellular and Environmental Regulation, of Photosynthesis. Oxford: Blackwell Scientific Publications.

Friso, G., Majeran, W., Huang, M., Sun, Q., & van Wijk, K. J. (2010). Reconstruction of metabolic pathways, protein expression, and homeostasis machineries across maize bundle sheath and mesophyll chloroplasts: large-scale quantitative proteomics using the first maize genome assembly. *Plant physiology*, *152*(3), 1219–1250. https://doi.org/10.1104/pp.109.152694

Fuchs, P., Rugen, N., Carrie, C., Elsässer, M., Finkemeier, I., Giese, J., Hildebrandt, T. M., Kühn, K., Maurino, V. G., Ruberti, C., Schallenberg-Rüdinger, M., Steinbeck, J., Braun, H. P., Eubel, H., Meyer, E. H., Müller-Schüssele, S. J., & Schwarzländer, M. (2020). Single organelle function and organization as estimated from Arabidopsis mitochondrial proteomics. *The Plant journal : for cell and molecular biology*, *101*(2), 420–441. https://doi.org/10.1111/tpj.14534

Furbank R. T. (2011). Evolution of the C(4) photosynthetic mechanism: are there really three C(4) acid decarboxylation types?. *Journal of experimental botany*, *62*(9), 3103–3108. https://doi.org/10.1093/jxb/err080

Ghannoum O, Evans JR, Caemmerer S (2011) Nitrogen and water use efficiency of C4 plants. In: C4 photosynthesis and related CO2 concentrating mechanisms. Raghavendra AS, Sage RF (eds.), Springer Netherlands: 129–146. http://dx.doi.org/10.1007/978-90-481-9407-0

Gerrard Wheeler, M. C., Tronconi, M. A., Drincovich, M. F., Andreo, C. S., Flügge, U. I., & Maurino, V. G. (2005). A comprehensive analysis of the NADP-malic enzyme gene family of Arabidopsis. *Plant physiology*, *139*(1), 39–51. https://doi.org/10.1104/pp.105.065953

Grover, S. D., Canellas, P. F., & Wedding, R. T. (1981). Purification of NAD malic enzyme from potato and investigation of some physical and kinetic properties. *Archives of biochemistry and biophysics*, *209*(2), 396–407. https://doi.org/10.1016/0003-9861(81)90297-6

Hatch MD (1987) C4 photosynthesis: a unique blend of modified biochemistry, anatomy and ultrastructure. Biochim.Biophys. Acta 895: 81–106. https://doi.org/10.1023/A:1020471718805

Heimann L, Horst I, Perduns R, Dreesen B, Offermann S, Peterhänsel C (2013) A common histone modification code on C4 genes in maize and its conservation in *Sorghum bicolor* and *Setaria italica*. Plant Physiol. 162: 456–469. https://doi.org/10.1104/pp.113.216721

Howe KL, Contreras-Moreira B, De Silva N, Maslen G, Akanni W, Allen J, Alvarez-Jarreta J, Barba M, Bolser DM, Cambell L, Carbajo M, Chakiachvili M, Christensen M, Cummins C, Cuzick A, Davis P, Fexova S, Gall A, George N, Gil L, Gupta P, Hammond-Kosack KE, Haskell E, Hunt SE, Jaiswal P, Janacek SH, Kersey PJ, Langridge N, Maheswari U, Maurel T, McDowall MD, Moore B, Muffato M, Naamati G, Naithani S, Olson A, Papatheodorou I, Patricio M, Paulini M, Pedro H, Perry E, Preece J, Rosello M, Russell M, Sitnik V, Staines DM, Stein J, Tello-Ruiz MK, Trevanion SJ, Urban M, Wei S, Ware D, Williams G, Yates AD, Flicek P (2020) Ensembl Genomes 2020-enabling non-vertebrate genomic research. Nucleic Acids Res. 48, D689–D695. https://doi.org/10.1093/nar/gkz890

John, C. R., Smith-Unna, R. D., Woodfield, H., Covshoff, S., & Hibberd, J. M. (2014). Evolutionary convergence of cell-specific gene expression in independent lineages of C4 grasses. *Plant physiology*, *165*(1), 62–75. https://doi.org/10.1104/pp.114.238667

Jordan DB, Ogren WL (1984) The CO2/O2 specificity of ribulose 1,5-bisphosphate carboxylase/oxygenase. Planta 161: 308–313. https://doi.org/10.1007/BF00398720

Kao, Y. T., Gonzalez, K. L., & Bartel, B. (2018). Peroxisome Function, Biogenesis, and Dynamics in Plants. *Plant physiology*, *176*(1), 162–177. https://doi.org/10.1104/pp.17.01050

Kinsella, R. J., Kähäri, A., Haider, S., Zamora, J., Proctor, G., Spudich, G., Almeida-King, J., Staines, D., Derwent, P., Kerhornou, A., Kersey, P., & Flicek, P. (2011). Ensembl BioMarts: a hub for data retrieval across taxonomic space. *Database : the journal of biological databases and curation*, *2011*, bar030. https://doi.org/10.1093/database/bar030

Laemmli U. K. (1970). Cleavage of structural proteins during the assembly of the head of bacteriophage T4. *Nature*, *227*(5259), 680–685. https://doi.org/10.1038/227680a0

Leonardi, G., Carlos, N. A., Mazzafera, P., & Balbuena, T. S. (2015). Eucalyptus urograndis stem proteome is responsive to short-term cold stress. *Genetics and molecular biology*, *38*(2), 191–198. https://doi.org/10.1590/S1415-475738220140235

Lichtenthaler HK, Schwender J, Disch A, Rohmer M (1997) Biosynthesis of isoprenoids in higher plant chloroplast proceed via a mevalonate-independent pathway. FEBS Lett. 400: 271–274. https://doi.org/10.1016/S0014-5793(96)01404-4

Ludwig M. (2016). The Roles of Organic Acids in C4 Photosynthesis. *Frontiers in plant science*, *7*, 647. https://doi.org/10.3389/fpls.2016.00647

Lundgren, M. R., Osborne, C. P., & Christin, P. A. (2014). Deconstructing Kranz anatomy to understand C4 evolution. *Journal of experimental botany*, *65*(13), 3357–3369. https://doi.org/10.1093/jxb/eru186

Maier, A., Zell, M. B., & Maurino, V. G. (2011). Malate decarboxylases: evolution and roles of NAD(P)-ME isoforms in species performing C(4) and C(3) photosynthesis. *Journal of experimental botany*, *62*(9), 3061–3069. https://doi.org/10.1093/jxb/err024

Majeran, W., Friso, G., Ponnala, L., Connolly, B., Huang, M., Reidel, E., Zhang, C., Asakura, Y., Bhuiyan, N. H., Sun, Q., Turgeon, R., & van Wijk, K. J. (2010). Structural and metabolic transitions of C4 leaf development and differentiation defined by microscopy and quantitative proteomics in maize. *The Plant cell*, *22*(11), 3509–3542. https://doi.org/10.1105/tpc.110.079764

Mamidi, S., Healey, A., Huang, P. et al. (2020) A genome resource for green millet Setaria viridis enables discovery of agronomically valuable loci. Nat Biotechnol 38, 1203–1210. https://doi.org/10.1038/s41587-020-0681-2

Meister, M, Agostino, A, Hatch, MD (1996) The roles of malate and aspartate in C4 photosynthetic metabolism of Flaveria bidentis (L.). Planta 199, 262–269. https://doi.org/10.1007/BF00196567

Mueller, N. D., Gerber, J. S., Johnston, M., Ray, D. K., Ramankutty, N., & Foley, J. A. (2012). Closing yield gaps through nutrient and water management. *Nature*, *490*(7419), 254–257. https://doi.org/10.1038/nature11420

Pan, R., & Hu, J. (2018). Proteome of Plant Peroxisomes. *Sub-cellular biochemistry*, *89*, 3–45. https://doi.org/10.1007/978-981-13-2233-4_1

Pick, T. R., Bräutigam, A., Schlüter, U., Denton, A. K., Colmsee, C., Scholz, U., Fahnenstich, H., Pieruschka, R., Rascher, U., Sonnewald, U., & Weber, A. P. (2011). Systems analysis of a maize leaf developmental gradient redefines the current C4 model and provides candidates for regulation. *The Plant cell*, *23*(12), 4208–4220. https://doi.org/10.1105/tpc.111.090324

Rao, X., Lu, N., Li, G., Nakashima, J., Tang, Y., & Dixon, R. A. (2016). Comparative cell-specific transcriptomics reveals differentiation of C4 photosynthesis pathways in switchgrass and other C4 lineages. *Journal of experimental botany*, *67*(6), 1649–1662. https://doi.org/10.1093/jxb/erv553

Reiner, A., Yekutieli, D., & Benjamini, Y. (2003). Identifying differentially expressed genes using false discovery rate controlling procedures. *Bioinformatics (Oxford, England)*, *19*(3), 368–375. https://doi.org/10.1093/bioinformatics/btf877

Sage R. F. (2004). The evolution of C_4 photosynthesis. *The New phytologist*, *161*(2), 341–370. https://doi.org/10.1111/j.1469-8137.2004.00974.x

Sage, R. F., Sage, T. L., & Kocacinar, F. (2012). Photorespiration and the evolution of C4 photosynthesis. *Annual review of plant biology*, *63*, 19–47. https://doi.org/10.1146/annurev-arplant-042811-105511

Saigo, M., Alvarez, C. E., Andreo, C. S., & Drincovich, M. F. (2013). Plastidial NADP-malic enzymes from grasses: unraveling the way to the C4 specific isoforms. *Plant physiology and biochemistry : PPB*, *63*, 39–48. https://doi.org/10.1016/j.plaphy.2012.11.009

Saigo, M., Bologna, F. P., Maurino, V. G., Detarsio, E., Andreo, C. S., & Drincovich, M. F. (2004). Maize recombinant non-C4 NADP-malic enzyme: a novel dimeric malic enzyme with high specific activity. *Plant molecular biology*, *55*(1), 97–107. https://doi.org/10.1007/s11103-004-0472-z

Saigo M, Tronconi MA, Gerrard Wheeler MC, Alvarez CE, Drincovich MF, Andreo CS (2013b) Biochemical approaches to C4 photosynthesis evolution studies: the case of malic enzymes decarboxylases. Photosynth. Res. 117: 177–187. https://doi.org/10.1007/s11120-013-9879-1.

Schlüter, U., & Weber, A. (2020). Regulation and Evolution of C_4 Photosynthesis. *Annual review of plant biology*, *71*, 183–215. https://doi.org/10.1146/annurev-arplant-042916-040915

Schulze ED, Hall AE (1982) Stomatal responses, water loss and CO2 assimilation rates of plants in contrasting environments. In: Physiological plant ecology II: water relations and carbon assimilation. Lange OL, Nobel PS, Osmond CB, Ziegler H (eds), Springer-Verlag: 181–230.

Schwacke, R., Ponce-Soto, G. Y., Krause, K., Bolger, A. M., Arsova, B., Hallab, A., Gruden, K., Stitt, M., Bolger, M. E., & Usadel, B. (2019). MapMan4: A Refined Protein Classification and Annotation Framework Applicable to Multi-Omics Data Analysis. *Molecular plant*, *12*(6), 879–892. https://doi.org/10.1016/j.molp.2019.01.003

Shih, P. M., Occhialini, A., Cameron, J. C., Andralojc, P. J., Parry, M. A., & Kerfeld, C. A. (2016). Biochemical characterization of predicted Precambrian RuBisCO. *Nature communications*, *7*, 10382. https://doi.org/10.1038/ncomms10382

Soll, J., Schultz, G., Rüdiger, W., & Benz, J. (1983). Hydrogenation of geranylgeraniol : two pathways exist in spinach chloroplasts. *Plant physiology*, *71*(4), 849–854. https://doi.org/10.1104/pp.71.4.849

Storey, J. D., & Tibshirani, R. (2003). Statistical significance for genomewide studies. *Proceedings of the National Academy of Sciences of the United States of America*, *100*(16), 9440–9445. https://doi.org/10.1073/pnas.1530509100

Sweetlove, L. J., Beard, K. F., Nunes-Nesi, A., Fernie, A. R., & Ratcliffe, R. G. (2010). Not just a circle: flux modes in the plant TCA cycle. *Trends in plant science*, *15*(8), 462–470. https://doi.org/10.1016/j.tplants.2010.05.006

Titus, D. E., & Becker, W. M. (1985). Investigation of the glyoxysome-peroxisome transition in germinating cucumber cotyledons using double-label immunoelectron microscopy. *The Journal of cell biology*, *101*(4), 1288–1299. https://doi.org/10.1083/jcb.101.4.1288

Tronconi, M. A., Andreo, C. S., & Drincovich, M. F. (2018). Chimeric Structure of Plant Malic Enzyme Family: Different Evolutionary Scenarios for NAD- and NADP-Dependent Isoforms. *Frontiers in plant science*, *9*, 565. https://doi.org/10.3389/fpls.2018.00565

Tronconi, M. A., Fahnenstich, H., Gerrard Weehler, M. C., Andreo, C. S., Flügge, U. I., Drincovich, M. F., & Maurino, V. G. (2008). Arabidopsis NAD-malic enzyme functions as a homodimer and heterodimer and has a major impact on nocturnal metabolism. *Plant physiology*, *146*(4), 1540–1552. https://doi.org/10.1104/pp.107.114975

Tronconi, M. A., Gerrard Wheeler, M. C., Maurino, V. G., Drincovich, M. F., & Andreo, C. S. (2010). NAD-malic enzymes of Arabidopsis thaliana display distinct kinetic mechanisms that support differences in physiological control. *The Biochemical journal*, *430*(2), 295–303. https://doi.org/10.1042/BJ20100497

Tronconi, M. A., Hüdig, M., Schranz, M. E., & Maurino, V. G. (2020). Independent Recruitment of Duplicated β-Subunit-Coding NAD-ME Genes Aided the Evolution of C4 Photosynthesis in Cleomaceae. *Frontiers in plant science*, *11*, 572080. https://doi.org/10.3389/fpls.2020.572080

Tronconi, M. A., Maurino, V. G., Andreo, C. S., & Drincovich, M. F. (2010). Three different and tissue-specific NAD-malic enzymes generated by alternative subunit association in Arabidopsis thaliana. *The Journal of biological chemistry*, *285*(16), 11870–11879. https://doi.org/10.1074/jbc.M109.097477

Tyanova, S., Temu, T., Sinitcyn, P., Carlson, A., Hein, M. Y., Geiger, T., Mann, M., & Cox, J. (2016). The Perseus computational platform for comprehensive analysis of (prote)omics data. *Nature methods*, *13*(9), 731–740. https://doi.org/10.1038/nmeth.3901

Van Eck J. (2018). The Status of *Setaria viridis* Transformation: *Agrobacterium*-Mediated to Floral Dip. *Frontiers in plant science*, *9*, 652. https://doi.org/10.3389/fpls.2018.00652

Van Eck, J., & Swartwood, K. (2015). Setaria viridis. *Methods in molecular biology (Clifton, N.J.)*, *1223*, 57–67. https://doi.org/10.1007/978-1-4939-1695-5_5

Vranová, E., Coman, D., & Gruissem, W. (2013). Network analysis of the MVA and MEP pathways for isoprenoid synthesis. *Annual review of plant biology*, *64*, 665–700. https://doi.org/10.1146/annurev-arplant-050312-120116

Wang L, Wang C, Liu X, Cheng J, Li S, Zhu JK, Gong Z (2019) Peroxisomal β-oxidation regulates histone acetylation and DNA methylation in *Arabidopsis*. Proc. Natl. Acad. Sci. USA 116: 10576–10585. https://doi.org/10.1073/pnas.1904143116

Wang, X., Gowik, U., Tang, H., Bowers, J. E., Westhoff, P., & Paterson, A. H. (2009). Comparative genomic analysis of C4 photosynthetic pathway evolution in grasses. *Genome biology*, *10*(6), R68. https://doi.org/10.1186/gb-2009-10-6-r68

Wang, Y., Bräutigam, A., Weber, A. P., & Zhu, X. G. (2014). Three distinct biochemical subtypes of C4 photosynthesis? A modelling analysis. *Journal of experimental botany*, *65*(13), 3567–3578. https://doi.org/10.1093/jxb/eru058

Washburn, J. D., Schnable, J. C., Conant, G. C., Brutnell, T. P., Shao, Y., Zhang, Y., Ludwig, M., Davidse, G., & Pires, J. C. (2018). Genome-Guided Phylo-Transcriptomic Methods and the Nuclear Phylogenetic Tree of the Paniceae Grasses. *Scientific reports*, *8*(1), 7120. https://doi.org/10.1038/s41598-018-25620-4

Watson-Lazowski, A., Papanicolaou, A., Sharwood, R., & Ghannoum, O. (2018). Investigating the NAD-ME biochemical pathway within C_4 grasses using transcript and amino acid variation in C_4 photosynthetic genes. *Photosynthesis research*, *138*(2), 233–248. https://doi.org/10.1007/s11120-018-0569-x

Weiner, H., Heldt, H.W. Inter- and intracellular distribution of amino acids and other metabolites in maize (Zea mays L.) leaves. Planta 187, 242–246 (1992). https://doi.org/10.1007/BF00201946

Figure legends

Figure 1: Schematic model of the C_4 photosynthesis pathway. In C_4 plants photosynthetic reactions are distributed between two cell types. Carbon is initially fixed into C_4 acids within mesophyll cells and then these compounds are transported to the bundle sheath cells, where they undergo decarboxylation generating CO_2 to be incorporated into the Calvin cycle. This cycle produces an enrichment in CO_2 of the RuBisCO environment, thus reducing its oxygenase activity. Names in black correspond to metabolites: CO_2: carbon dioxide; HCO_3^-: bicarbonate; C_4: 4-carbon acid; C_3: 3-carbon acid; PEP: phosphoenolpyruvate; RuBP: ribulose-1,5-bisphosphate; PGA: 3-phosphoglyceric acid. Names in red correspond to C_4 genes: CA: carbonic anhydrase; PEPC: phosphoenolpyruvate carboxylase; PPDK: pyruvate/orthophosphate dikinase; NAD(P)-ME: NAD-dependent malic or NADP-dependent enzyme; PEPCK: phosphoenolpyruvate carboxykinase.

Figure 2: Protein distribution in M and BS from Setaria leaves. Volcano plot showing the proteins that were differentially enriched in M or in BS (light red). The horizontal line marks the limit of *p*-value<0.05, while the vertical lines mark the limit at which the difference in the proteins is more than doubled in one condition over the other **(A)**. Proteins identified according to their role, grouped by metabolism. Proteins significantly enriched in M or BS, showing these cells fulfil different functions in metabolic and regulatory processes **(B)**.

Figure 3: Kinetic and regulatory properties of Setaria C_4-NADP-ME. NADP-ME activity was determined at different malate concentrations, at pH 8.0 and 7.0. The activity unit s^{-1} corresponds to µmol of product generated per µmol of enzyme per second.

Figure 4: Regulatory properties of recombinant NAD-ME1 (A) and NAD-ME2 (B). The results represent the % of activity in the presence of each effector in relation to the activity measured in the absence of the metabolites (100%). Assays were performed by triplicate, and error bars indicate S.D. Red striped bars indicate inhibition (less than 70% residual activity), green bars indicate activation (more than 140%) and grey dotted bars indicate no significant change. Schematic representation showing that NAD-ME activity and Mal availability can be readily coordinated by the ratio of α-KG/Glu **(C)**.

Figure 5: Schematic model of the C_4 cycle in *S. viridis*. Besides the primary route of Mal decarboxylation in chloroplasts of BS cells (solid lines), a secondary route in the mitochondria (dashed lines) could also contribute to the C_4 carbon shuttle. The pyruvate generated in the mitochondria of BS would not be oxidised to form Acetyl-CoA, while in M several Pyr-independent pathways of Acetyl-CoA generation would be enhanced. In both cases, the Pyr pool would be preserved to maintain the C_4 shuttle. Additionally, in M chloroplasts the down-regulation of the shikimate pathway would reserve PEP molecules for PEPC primary carboxylation reactions.

Tables

		Transcripts ([a]John *et al.*, 2014; [b]Chang *et al.*, 2012)		Proteins ([c]this work; [d]Friso *et al.*, 2010)	
	ID	$Log_2FC(BS/M)$	*p-adjusted*	$Log_2FC(BS/M)$	*p-adjusted*
SvNAD-ME1	Sevir.2G333400	0.7434[a]	2.74E-03[a]	0.8267[c]	4.65E-02[c]
SvNAD-ME2	Sevir.9G199800	0.8385[a]	6.34E-04[a]	0.8735[c]	8.81E-02[c]
SvNADP-ME4 (C4)	Sevir.5G132500	7.2049[a]	7.82E-84[a]	5.4296[c]	3.34E-05[c]
ZmNAD-ME1	GRMZM2G085747	1.5706[b]	5.46E-13[b]	NA	NA
ZmNAD-ME2	GRMZM2G406672	3.4952[b]	4.93E-38[b]	NA	NA
ZmNADP-ME (C4)	GRMZM2G085019	6.6616[b]	1.20E-149[b]	1.48[d*]	9.13E-03[d]*
ZmNADP-ME (non-C4)	GRMZM2G122479	NA	NA	1.48[d*]	9.13E-03[d]*

Table 1: Convergence of NADP-ME and NAD-ME transcripts and proteins in *Setaria viridis* (Sv) and maize (Zm). Log_2FC (BS/M) of maize transcripts and proteins were obtained from Chang *et al.*, 2012 and Friso *et al*, 2010, respectively. Log_2FC (BS/M) of Setaria transcripts and proteins were obtained from John *et al.*, 2014 and this work, respectively. NA: not available.

	Zmnon-C_4	Sbnon-C_4	SetariaC_4	ZmC_4	SbC_4
Optimal pH	8.0	8.0	8.0	8.0	8.0
k_{cat} (s^{-1})	26.3	26.4	35.0	28.1	36.8
$S_{0,5}$ $NADP^+$ (µM)	70.2	16.8	9.3	8.0	11.0
$S_{0,5}$ Mal (mM)	0.8	0.6	0.18	0.2	0.4
Inhibition by Mal at pH 7.0	low	low	yes	yes	yes

Table 2: Kinetic parameters of Setaria chloroplastic NADP-ME. Maize (Zm) and sorghum (Sb) C_4 and non-C_4 enzyme parameters were previously determined and included for comparison (Detarsio *et al.*, 2003; Saigo *et al.*, 2004; Detarsio *et al.*, 2007; Saigo *et al.*, 2013a). *k*cat corresponds to the µmol of substrate converted into product by s under optimal conditions per µmol of active site and $S_{0.5}$ is the substrate concentration for which half of maximum reaction rate is obtained. %CV were below 5%.

	SetariaNAD-ME1	SetariaNAD-ME2	AtNAD-ME1	AtNAD-ME2
Optimal pH	6.5	6.5	6.4	6.6
k_{cat} (s^{-1})	12.7	15.5	31.1	44.1
$S_{0,5}$ NAD^+ (mM)	1.8	0.5	0.5	0.5
$S_{0,5}$ Mal (mM)	3.9	3.4	3.0	3.0

Table 3: Comparative summary of the most important biochemical characteristics of Setaria NAD-MEs. Arabidopsis (At) NAD-ME parameters (Tronconi *et al*., 2008) were included for comparison. *k*cat corresponds to the µmol of substrate converted into product by s under optimal conditions per µmol of active site and $S_{0.5}$ is the substrate concentration for which half of maximum reaction rate is obtained. %CV were below 5%.

Protein	Sevir gene identifier	Description	Cell Type	FC BS/M	log_2FC BS/M	FDR-*p*
		CHLOROPLAST				
DXP	Sevir.5G070600	1-deoxy-D-xylulose 5-phosphate reductoisomerase	M	0.10	-3.31	2.41E-04
GSA	Sevir.3G199700	glutamate-1-semialdehyde aminotransferase	BS	4.52	2.18	1.53E-03
CHLI1	Sevir.7G301900	magnesium-chelatase subunit I	BS	3.43	1.78	1.53E-03
CHLM	Sevir.4G021700	magnesium-protoporphyrin O-methyltransferase	BS	2.35	1.23	4.13E-04
CRD1	Sevir.5G037900	magnesium-protoporphyrin IX monomethyl ester cyclase	BS	10.59	3.41	4.06E-03
DHQS	Sevir.2G301400	3-dehydroquinate synthase	BS	4.59	2.20	1.77E-02
DHQ-SDH	Sevir.3G361900	bifunctional 3-dehydroquinate dehydratase/shikimate dehydrogenase	BS	2.13	1.09	2.21E-02
SKL1	Sevir.3G344100	shikimate kinase	BS	4.17	2.06	2.21E-04
CS2	Sevir.9G469600	chorismate synthase 2	BS	4.52	2.18	2.15E-02
ADT6	Sevir.2G137000	Arogenate dehydratase	BS	3.64	1.87	7.92E-04
		MITOCHONDRIA				
IVD	Sevir.3G048300	isovaleryl-CoA-dehydrogenase	M	0.26	-1.95	7.87E-03
MCCB	Sevir.6G157100	3-methylcrotonyl-CoA carboxylase	M	0.25	-1.98	1.85E-02
FAH	Sevir.1G048700	fumarylacetoacetase	M	0.27	-1.91	6.43E-05
IDH1	Sevir.1G221900	isocitrate dehydrogenase 1	BS	2.08	1.06	5.60E-03
IDH1	Sevir.7G146600	isocitrate dehydrogenase 1	BS	4.83	2.27	8.81E-03
FUM2	Sevir.9G415100	fumarase 2	BS	2.10	1.07	6.21E-03
GDH1	Sevir.9G057100	glutamate dehydrogenase 1	BS	6.72	2.75	2.74E-04
GDH2	Sevir.7G196400	glutamate dehydrogenase 2	BS	39.65	5.31	1.23E-04
PHT3;1	Sevir.1G339000	phosphate transporter 3;1	BS	2.04	1.03	1.65E-02
BOU	Sevir.9G317900	mitochondrial substrate carrier family protein	BS	21.46	4.42	2.26E-03
ATP5	Sevir.1G297400	delta subunit of ATP synthase	BS	4.39	2.13	1.09E-04
petA	Sevir.7G087700	Ubiquinol-cytochrome C reductase iron-sulfur subunit	BS	3.98	1.99	1.33E-03
SLC 25A8_9	Sevir.8G262500	plant uncoupling mitochondrial protein 1	BS	2.11	1.08	4.10E-03
UQCRB	Sevir.9G045500	cytochrome bd ubiquinol oxidase, 14kDa subunit	BS	2.39	1.26	3.61E-03
MSD1	Sevir.3G294500	manganese superoxide dismutase 1	BS	7.20	2.85	3.58E-04
PRXIIF	Sevir.5G049000	peroxiredoxin IIF	BS	4.09	2.03	4.77E-04
PDHK	Sevir.2G418200	pyruvate dehydrogenase kinase	BS	2.67	1.41	2.11E-03
		PEROXISOME				

ACX1	Sevir.4G062700	acyl-CoA oxidase 1	M	0.35	-1.52	2.52E-04
MFP2	Sevir.5G161600	multifunctional protein 2/3-hydroxyacyl-CoA dehydrogenase	M	0.32	-1.65	3.13E-02
KAT2	Sevir.1G372900	peroxisomal 3-ketoacyl-CoA thiolase 3	M	0.39	-1.36	9.90E-03
CAT1	Sevir.1G116500	catalase 1	M	0.08	-3.58	5.86E-04
CAT2	Sevir.4G299100	catalase 2	M	0.30	-1.72	3.77E-02
GR1	Sevir.1G368300	glutathione-disulfide reductase	M	0.30	-1.75	6.35E-04
MDAR1	Sevir.2G138000	monodehydroascorbate reductase 1	M	0.43	-1.23	5.82E-02
PMDH1	Sevir.3G419600	NAD-malate dehydrogenase 1	M	0.39	-1.36	9.00E-03
CSY3	Sevir.1G026500	citrate synthase 3	M	0.41	-1.30	6.84E-04
AACT	Sevir.7G290900	Acetoacetyl-CoA thiolase	M	0.39	-1.35	5.19E-04
IDI2	Sevir.2G354200	isopentenyl pyrophosphate:dimethylallyl pyrophosphate isomerase 2	M	0.23	-2.13	1.19E-03

Table 4: Experimental data corresponding to the proteins enriched in either M or BS. The table shows the summary of the results of the group of proteins mentioned in the text. The putative subcellular location of each protein was inferred by the identification of its ortholog in proteomic databases of maize chloroplasts (Friso et al., 2010), Arabidopsis mitochondria (Fuchs et al., 2020) and Arabidopsis peroxisomes (Pan and Hu, 2018). Chloroplastic or mitochondrial location was also predicted by TargetP.

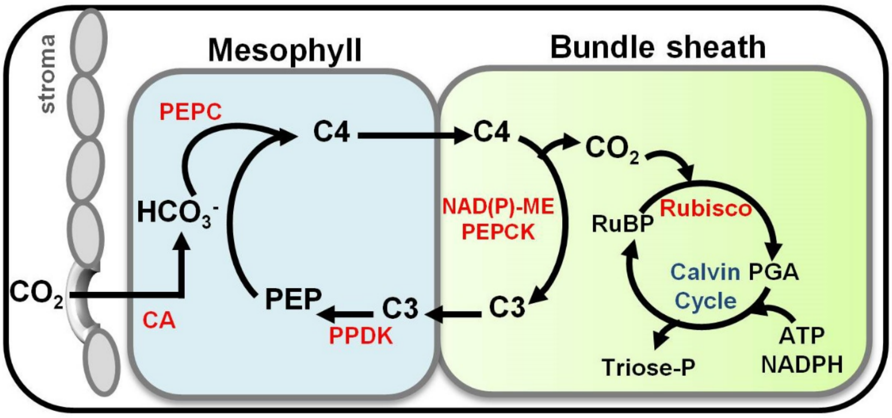

Figure 1: Schematic model of the C_4 photosynthesis pathway. In C_4 plants the photosynthetic reactions are distributed between two cell types, they initially fix the carbon to C_4 acids within the mesophyll cells and then transport these compounds to the bundle sheath cells, where they are decarboxylated so that the resulting CO_2 is incorporated into the Calvin cycle. This cycle produces the enrichment of the RuBisCO environment in CO_2, thus reducing its oxygenase activity. Names in black correspond to metabolites; CO_2: carbon dioxide; HCO_3^-: bicarbonate; C_4: 4-carbon acid; C_3: 3-carbon acid; PEP: phosphoenolpyruvate; RuBP: ribulose-1,5-bisphosphate; PGA: 3-phosphoglyceric acid. Names in red correspond to C_4 genes; CA: carbonic anhydrase; PEPC: phosphoenolpyruvate carboxylase; PPDK: pyruvate/orthophosphate dikinase; NAD(P)-ME: NAD-dependent malic or NADP-dependent enzyme; PEPCK: phosphoenolpyruvate carboxykinase.

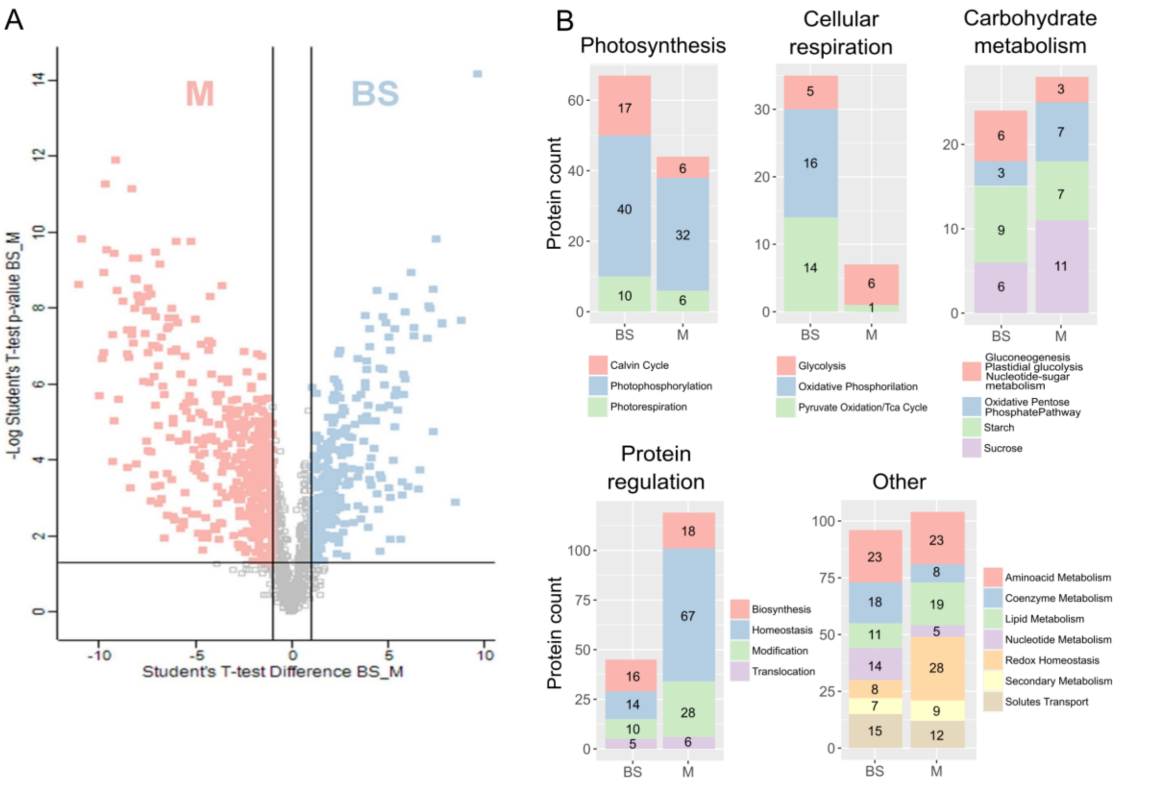

Figure 2: Protein distribution in M and BS from Setaria leaves. Volcano plot showing the proteins that were differentially enriched in M or in BS (light red). The horizontal line marks the limit of *p*-value<0.05, while the vertical lines mark the limit at which the difference in the proteins is more than doubled in one condition over the other **(A)**. Proteins identified according to their role, grouped by metabolism. Proteins significantly enriched in M or BS show that these cells fulfil different functions in metabolic and regulatory processes **(B)**.

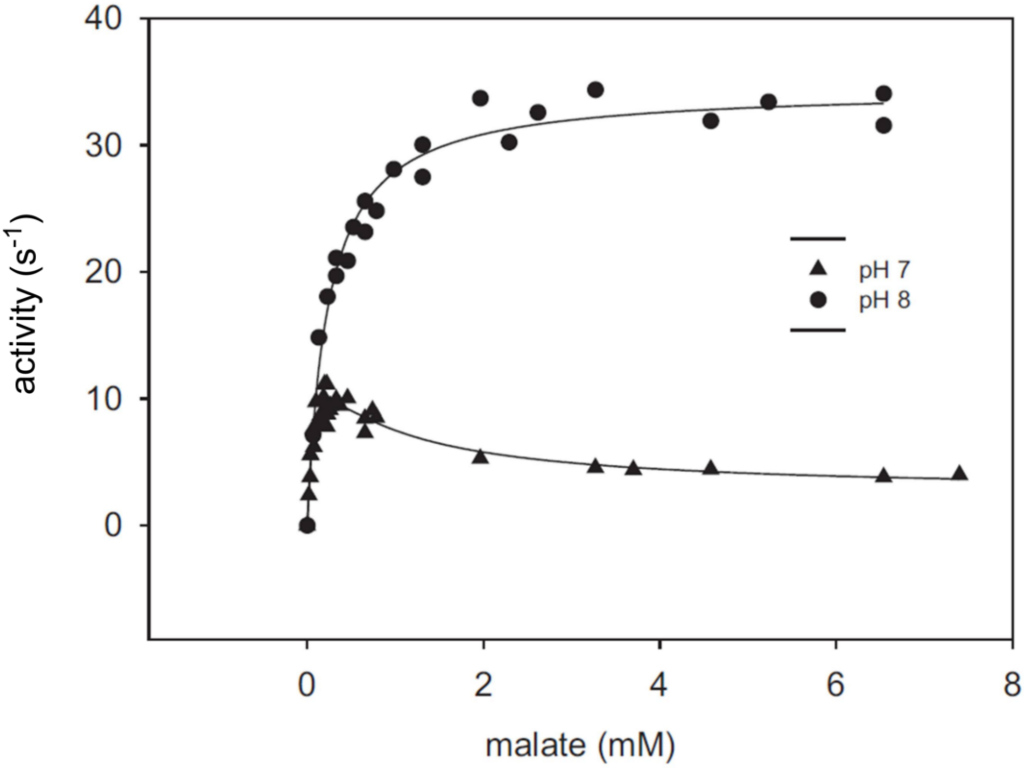

Figure 3: Kinetic and regulatory properties of Setaria C_4-NADP-ME. NADP-ME activity was determined at different malate concentrations, at pH 8.0 and 7.0. The activity unit s^{-1} corresponds to µmol of product generated per µmol of enzyme per second.

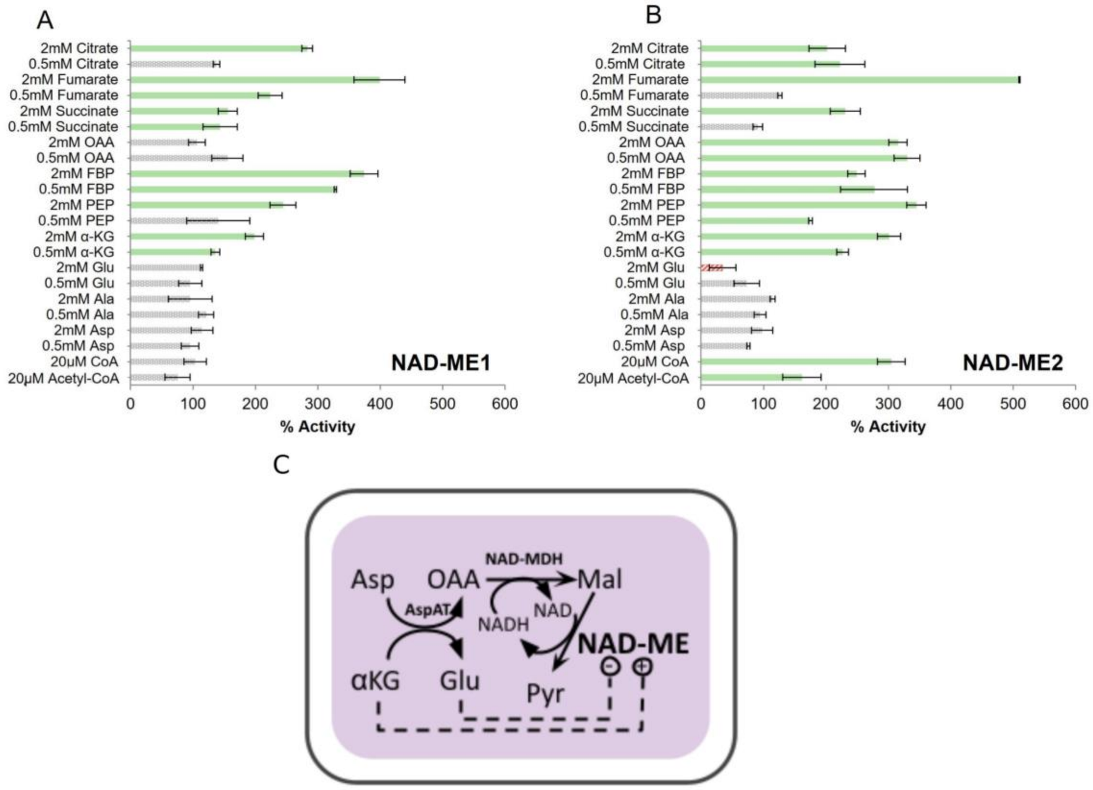

Figure 4: Regulatory properties of recombinant NAD-ME1 (A) and NAD-ME2 (B). The results represent the % of activity in the presence of each effector in relation to the activity measured in the absence of the metabolites (100%). Assays were performed by triplicate, and error bars indicate S.D. Red striped bars indicate inhibition (less than 70% residual activity), green bars indicate activation (more than 140%) and grey dotted bars indicate no significant change. Schematic representation showing that NAD-ME activity and Mal availability can be readily coordinated by the ratio of α-KG/Glu (C)

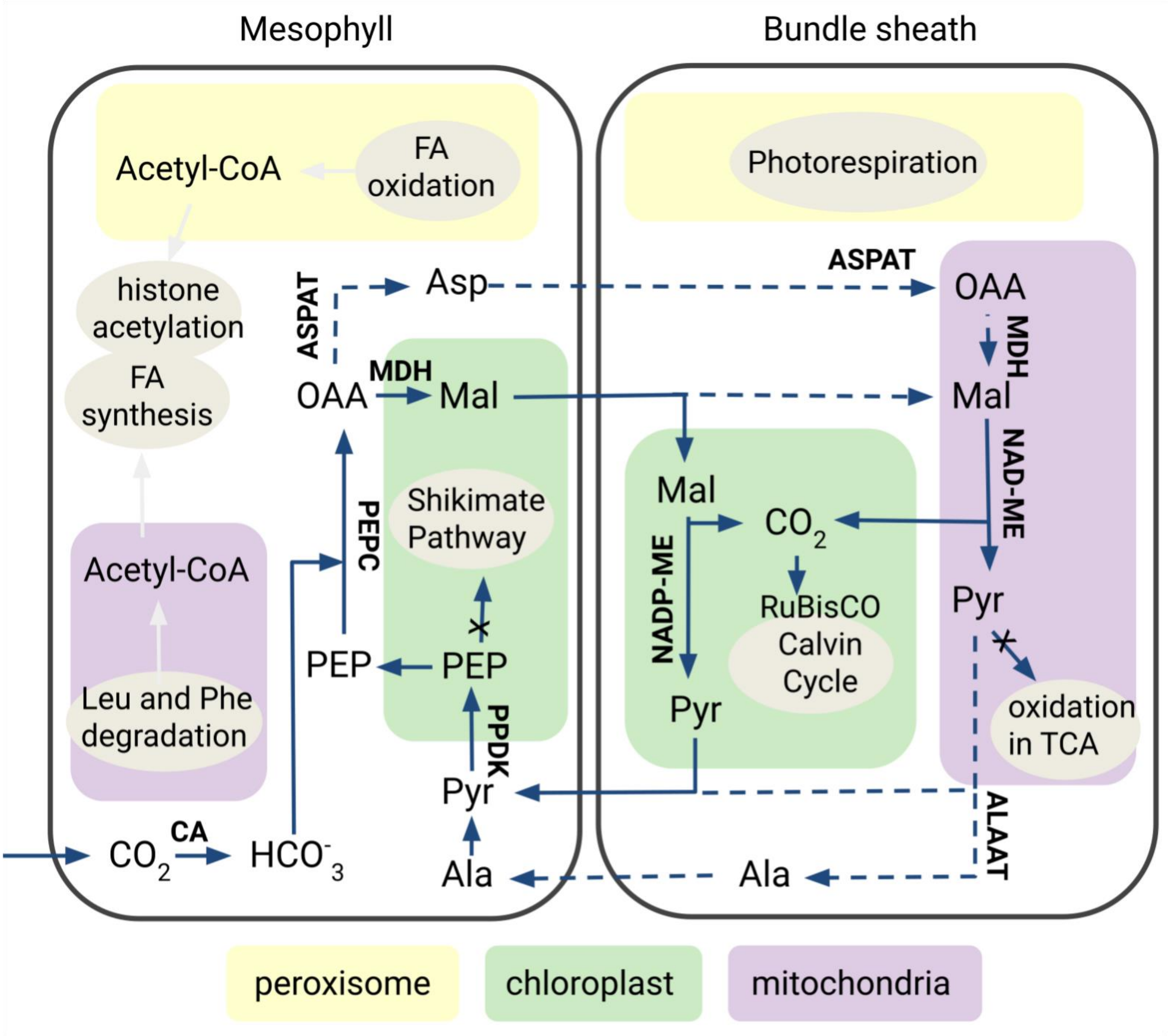

Figure 5: Schematic model of the C_4 cycle in *S. viridis*. Besides the primary route of Mal decarboxylation in chloroplasts of BS cells (solid lines), a secondary route in the mitochondria (dashed lines) could also contribute to the C_4 carbon shuttle. The pyruvate generated in the mitochondria of BS would not be oxidized to form Acetyl-CoA, while in M several Pyr-independent pathways of Acetyl-CoA generation are enhanced. In both cases, the Pyr pool would be preserved to maintain the C_4 shuttle. Additionally, in M chloroplasts the down-regulation of the shikimate pathway would reserve the PEP for the primary carboxylation by PEPC.